Resonant Photonic Structure in Porous Silicon for Biosensing

Yiliang Zhao[a], Gilberto A. Rodriguez[b], Yasmin M. Graham[c], Tengfei Cao[a], Girija Gaur[b], and Sharon M. Weiss*[a,b]

[a] Interdisciplinary Graduate Program in Materials Science, Vanderbilt University, Nashville, TN 37235, USA; [b] Department of Electrical Engineering and Computer Science, Vanderbilt University, Nashville, TN 37235, USA; [c] Department of Mechanical Engineering, University of Maryland Baltimore County, Baltimore, MD 21250, USA

ABSTRACT

The formation of resonant photonic structures in porous silicon leverages the benefit of high surface area for improved molecular capture that is characteristic of porous materials with the advantage of high detection sensitivity that is a feature of resonant optical devices. This review provides an overview of the biosensing capabilities of a variety of resonant porous silicon photonic structures including microcavities, Bloch surface waves, ring resonators, and annular Bragg resonators. Detection sensitivities > 1000 nm/RIU are achieved for small molecule detection. The challenge of detecting molecules that approach and exceed the pore diameter is also addressed.

Keywords: porous silicon, microcavity, Bloch surface wave, microring, resonator, biosensor

1. INTRODUCTION

Porous silicon (PSi) has attracted considerable interest for gas, chemical, and biomolecular sensing applications due to its large internal surface area, straightforward fabrication, and versatile surface chemistry.[1-3] In particular, its refractive index can be easily tuned, enabling the fabrication of numerous photonic structures including interferometers,[4] Bragg mirrors,[5] rugate filters,[6] microcavities,[7,8] waveguides,[9,10] Bloch surface wave (BSW) structures,[11,12] and microring and racetrack resonators.[13,14] The large surface area of PSi, arising from the presence of nanoscale pores, facilitates enhanced light-matter interaction (i.e., light-molecule interaction) in PSi optical structures, especially for those structures that support guided modes in the PSi film. It is well-known that enhanced light-matter interaction leads to improved sensitivity to biomolecule binding events.[15] For nonporous materials, the majority of the active sensing region that spatially overlaps with guided modes is inaccessible to molecules as it resides inside a solid material; molecules can only interact with an evanescent field at the sensor surface.[16] In the case of PSi, molecules infiltrate the porous matrix and directly interact with a guided mode. The effective index of the guided mode is greatly perturbed by the addition of molecules, changing the refractive index of the PSi according to the appropriate effective medium approximation.[17] While single layer PSi thin films and interferometers do enable a greater interaction between light and molecules compared to a nonporous thin film or interferometer, due to the larger number of molecules captured in the pores, resonant PSi optical structures further benefit from increased intensity of light within a guided mode layer, which also increases the detection sensitivity of optical structures. For small molecule detection, the resonant PSi waveguide has been reported to possess a detection sensitivity 10-40 times greater than a planar silicon-on-insulator (SOI) waveguide.[18]

This review focuses on recent advances in PSi optical structures. Several other reviews and papers broadly cover earlier work on PSi optical structures.[1,3,19-21] We begin with a discussion of the PSi microcavity. The microcavity consists of a pair of Bragg mirrors separated by a cavity layer deep within the structure. Although molecules are accessible to the entire porous structure, the sensor response is predominantly determined by the effective index change in the cavity layer. While the microcavity is among the most sensitive sensor platforms, the long required diffusion depth for molecules in high aspect ratio pores presents a challenge for molecules that are not significantly smaller than the pore diameter.[22] To overcome the mass transport challenge, an open-ended PSi membrane has been reported that allows molecules to flow through the pores in microfluidic-based assays and interact more favorably with the inner pore surface.[23] Next, we discuss a PSi-BSW sensor with an active sensing region at the surface of the structure that enables

*sharon.weiss@vanderbilt.edu; phone 1-615-343-8311; fax 1-615-343-6702

fast sensor response for the detection of both small and large molecules.[24] Third, we discuss the PSi ring resonator structure and its biosensing performance. Compact PSi ring resonators facilitate integration into on-chip silicon architectures. In comparison to traditional SOI ring resonators, the PSi ring resonator exhibits more than an order of magnitude increase in surface sensitivity for specific molecule detection.[13] Finally, we present progress on the development of PSi annular Bragg resonators (ABR) that support simple colorimetric detection, leading to a potentially portable, low-cost, and highly effective diagnostic solution.

2. BACKGROUND AND EXPERIMENTAL DETAILS

2.1 Microcavity

A one-dimensional multilayer microcavity is comprised of alternating layers of low and high refractive index possessing optical thicknesses corresponding to one fourth of the resonant wavelength (i.e., Bragg mirrors) and a central cavity layer with an optical thickness that is typically equivalent to one half the resonant wavelength of the microcavity. Light is localized in the central defect layer, making it the most sensitive region of the microcavity for detecting target analyte. The microcavity is one of the many PSi multilayer structures that can be straightforwardly fabricated by electrochemical etching with appropriate control of the applied current density. A high quality PSi microcavity requires several periods of alternating high and low porosity films, with the exact number of periods dependent on the refractive index contrast within the Bragg mirror layers. The reflectance spectrum of a microcavity is characterized by a resonance dip in the middle of a high reflectance band. Molecules captured in the microcavity lead to a shift of the resonance wavelength. In the work reviewed here, the wavelength shift is measured with a fiber-coupled Ocean Optics USB4000 CCD spectrometer. Reflectivity data are recorded continuously every 20 s with a spectral acquisition time of 10 ms over a wavelength range of 500 to 1000 nm.

2.2 Grating-coupled Bloch surface wave

The BSW structure is composed of periodic layers with alternating dielectric constant similar to a Bragg mirror, but its top layer is designed to be thinner to serve as a surface wave guiding layer. The electromagnetic field of a BSW mode is confined to the surface of the structure due to the activation of a defect surface state within photonic band gap and total internal reflection at the air interface.[25] In the work reviewed here, photoresist grating couplers are used to couple light into the BSW by providing the necessary mode matching through the generation of an appropriate diffracted mode. Angle resolved reflectance measurements of the BSW structures are performed in a Metricon 2010/M instrument, with a TE-polarized 1550 nm laser as the light source. At the proper coupling angle, a resonance peak appears in the reflectance spectrum. When small molecules infiltrate the PSi-BSW, the effective refractive index of the PSi layers increases, leading to a measureable shift in the resonance angles of the BSW, sub-surface wave(s), and band edge modes.[24] Large molecules bound on the surface of the BSW structure change the effective index of only the BSW mode and shift the its resonance angle. The active sensing region of the BSW is at the surface of the structure, facilitating a fast sensor response to molecular binding, but a reduced light-molecule interaction due to the reduced surface area available for molecular binding.

2.3 Ring resonator

The ring resonator configuration consists of a straight ridge waveguide in close proximity to a ring shaped waveguide. Transmitted light from the straight waveguide can couple into the ring at integer multiples of the optical path length of the ring following the relationship: $\lambda_{res} = \frac{2\pi r \cdot n_{eff}}{m}$, where λ_{res} is the resonance wavelength, r is the radius of the ring, n_{eff} is the effective index of the ring, and m is an integer.[26] Input light from the straight waveguide will couple to the ring at λ_{res} and will make multiple passes around the ring constructively interfering to create a strong locally confined field. The PSi ring resonator holds great promise as a biosensing platform for allowing direct interaction of infiltrated molecules with the resonant optical mode. In the work reviewed here, PSi ring resonator chips are cleaved to an approximate 2.5 mm waveguide length and placed on a piezo-controlled XYZ stage for measurement of transmission spectra. A TE-polarized tunable continuous wave laser (Santec TSL-510) is coupled into a tapered region of the PSi

straight ridge waveguide using lensed fiber. The laser is swept from 1500 to 1630 nm with step size of 0.05 nm. The transmitted light is detected using a fiber-coupled photodiode receiver (Newport 2936-C).

2.4 Annular Bragg resonator

While the microcavity structure discussed in Section 2.1 employs a linearly discrete refractive index profile on either side of the cavity, the ABR is based on a discrete refractive index profile that is positioned radially around the cavity region.[27] ABRs have been traditionally used to resonantly enhance the emission of light emitters incorporated in the cavity region.[28,29] By combining the enhanced emission properties supported by ABRs and the capability of PSi films to capture large quantities of molecular species inside the pores, PSi ABRs have the potential to be a highly efficiently platform for colorimetric biosensing. In the work presented here, colloidal quantum dots (QDs) are infiltrated into PSi-ABRs to achieve cavity modified QD emission with enhanced photoluminescence (PL) intensities as a first step toward colorimetric sensing. To quantify the QD emission, a Raman microscope (Thermo Scientific DXR) equipped with a 532 nm laser is used to excite the QDs embedded in PSi-ABRs and collect the fluorescence intensity over a wavelength range of 533 to 813 nm. For sensing operation, molecular binding events would lead to a resonance shift of the ABR and a concurrent color change in the ABR-modified QD emission. Hence, the presence of molecules could be determined by a simple color-change using a label-free sensing approach. Unlike former work in which QD-bioconjugates enables signal amplification in PSi biosensors,[30] here the QDs are separately infiltrated into the PSi and share the internal surface area with biomolecules.

2.5 PSi formation and lithographic process

The PSi structures are fabricated by electrochemical etching of *p*-type silicon wafers (<100>, 0.01-0.02 Ω·cm) in a 15% ethanoic hydrofluoric acid solution. Table 1 shows the current densities and etching times used to fabricate the structures discussed in this review. The microcavity (μc) has a configuration of $(L\ H)^9(H\ L)^9$, with H and L representing layers of high and low porosity, respectively. The PSi substrates used for the ABR and ring resonator both consist of a top high refractive index guiding layer and a bottom low refractive index cladding layer. The BSW structure consists of an 11 period multilayer with a very thin top defect layer (d_{BSW}) functioning as the surface guiding layer: $(d_{BSW})(L\ H)^{11}$. In order to facilitate molecule infiltration and attachment, the freshly etched samples for the fabrication of BSW and ring resonator structures are soaked in 1.5 mM KOH in ethanol for 5 min for pore widening. All samples are thermally oxidized. PSi layer thickness is estimated from scanning electron microscopy (SEM) images and the refractive indices are calculated by fitting reflectance spectra with transfer matrix simulations.

Table 1. Electrochemical etching parameters and physical characteristics of the PSi resonant structures discussed in this paper, where the layers are as defined in the main text.

Structure	Layer	Refractive Index	Current density (mA/cm^2)	Time (s)	Thickness (nm)
μC	H	1.35	48	6.1	125
	L	1.60	20	4.5	105
BSW	d_{BSW}	1.79	5	34	175
	H	1.24	48	22	580
	L	1.79	5	63	340
Ring	Guiding	1.79	5	114	600
	Cladding	1.24	48	53	1450
ABR	Top	1.60	20	23	500
	Cladding	1.30	70	32	600

In order to form the open-ended PSi microcavity for the comparison of analyte transport efficiency in on-substrate and membrane PSi structures, the microcavity structure is etched at the front side of a double side polished silicon wafer. Two high porosity sacrificial layers are included at the top and bottom of the microcavity to provide process tolerance and mechanical support. After thermal oxidation, aligned photolithography and reactive ion etching (RIE) are used to remove the silicon substrate at the backside.[23] The grating couplers on the BSW structures, the ABRs, and the ring resonators were patterned using standard electron beam lithography (EBL) and RIE as detailed in previous work.[13,24] Briefly, a layer of electron beam resist (ZEP-520A) is spun on the PSi substrates and patterned to serve as a mask for the RIE. The RIE then transfers the pattern into the top PSi layer and the residual resist is removed by oxygen plasma cleaning. Figure 1 shows SEM images of the fabricated PSi microcavity membrane, BSW, ring resonator, and ABR structures discussed in this review.

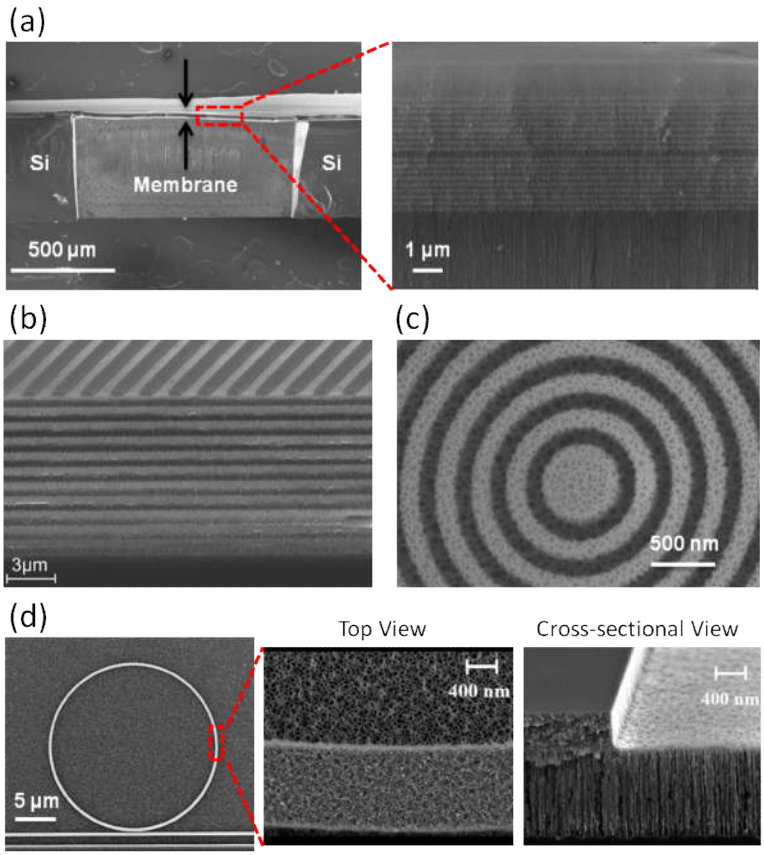

Figure 1. SEM images of (a) an open-ended PSi membrane. Magnified cross-sectional SEM shows the PSi layers comprising the microcavity and the surrounding sacrificial layers. Adapted with permission from Y. Zhao, G. Gaur, R. L. Mernaugh, P. E. Laibinis and S. M. Weiss, *Nanoscale Res. Lett.* 2016, 11, 395. Copyright 2016 Springer. (b) PSi-BSW structure with photoresist grating coupler. Adapted with permission from G. A. Rodriguez, J. D. Ryckman, Y. Jiao and S. M. Weiss, *Biosens. Bioelectron.* 2014, 53, 486. Copyright 2014 Elsevier B.V. (c) PSi-ABR. (d) PSi ring resonator, top view porosity profile of the waveguide and cladding layers, and cross section of the ridge waveguide after RIE. Adapted with permission from G. A. Rodriguez, S. Hu and S. M. Weiss, *Opt. Express* 2015, 23, 7111. Copyright 2015 Optical Society of America.

3. OPTICAL BIOSENSING

3.1 PSi microcavity membrane for efficient analyte transportation

PSi microcavities enable highly sensitive label-free optical sensing as a result of strong light-matter interaction between localized electric fields and target molecules captured in the central defect region.[17] However, the application of PSi microcavities as biosensors is challenged by an associated long response time due to hindered analyte diffusion in the

low porosity layers whose average pore size is smaller than 20 nm. Therefore, for the detection of large molecules whose sizes are on the same order as the pore diameter, the use of the PSi microcavity as a sensor platform becomes impractical. In order to improve molecule transport efficiency and reduce sensor response time, open-ended PSi membranes have been employed to realize a flow-through sensing scheme that allows analyte solutions to pass through the nanopores and interact more favorably with their inner surfaces.[23] The PSi membrane samples are sealed between two micro-channels with the same dimension. The upper channel contains the inlet for the analyte solution while outlet is present in the bottom channel, forcing the solution to pass through the open-ended pores (Figure 2a, b). The sensing performance of the PSi microcavity in both the flow-over (i.e., on-substrate) and flow-through (i.e., open-ended membrane) schemes were evaluated by detecting the specific binding of streptavidin to biotinylated PSi films. As shown in Figure 2c, the PSi microcavity membrane in the flow-through scheme saturates its response in approximately 25 min, while it takes over 2 h for the on-substrate PSi sensor in the flow-over scheme to reach saturation. This measurement indicates that the open-ended PSi membranes enable efficient analyte delivery and significantly reduce the sensor response time for protein detection.

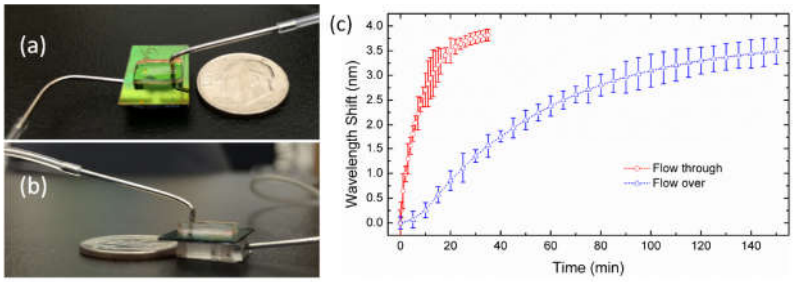

Figure 2. (a) Top and (b) plan views of the PSi microcavity membrane structure integrated with microfluidics. (c) Comparison of real-time sensor responses of flow-through PSi microcavity membrane and flow-over PSi microcavity upon exposure of sensor to a 5 μM streptavidin solution. Adapted with permission from Y. Zhao, G. Gaur, S. T. Retterer, P. E. Laibinis and S. M. Weiss, *Anal. Chem.* 2016, 88 (22), 10940. Copyright 2016 American Chemical Society.

3.2 PSi Bloch surface wave for size-selective detection

In addition to implementing flow-through sensing, the mass transport efficiency through porous films can also be improved by using sensors with strong light confinement close to the top surface. The PSi-BSW has the active sensing region at the surface of the structure, which facilitates molecule infiltration and promotes a fast sensor response to both small and large molecules.[24] The sensing performance of a grating-coupled BSW platform was tested upon exposure to large (> 10 nm) and small molecules (< 2 nm), as illustrated in Figure 3a. The chemical linkers, 3-aminopropyltrithoxysilane (3-APTES, 0.8 nm) and sulfosuccinimidyl-4-(N-maleimidomethyl) cyclohexane-1-carboxylate (sulfo-SMCC, 1.26nm), were attached to the PSi-BSW structures in succession as model small molecules. The attachment of these two small molecules prepares the surface for the immobilization of the chosen large molecule under test, a 13.2 nm long 40-mer thiol modified DNA that cannot efficiently infiltrate the ~20 nm pores of the high index PSi layers.[31] The resonance shift of the PSi-BSW structures in response to large and small molecule attachment are plotted in Figure 3b. The 3-APTES and sulfo-SMCC small molecules produce large resonance shifts (> 1 degree), indicating effective binding on the surface; the resonance shift of a sub-surface wave mode (not shown) further indicates that the small molecules can readily penetrate the porous matrix. The experimentally measured resonance shifts for the small molecule attachment in the PSi-BSW sensor correspond to an effective refractive index change of approximately $\Delta n = 0.03 - 0.05$ for 3-APTES and $\Delta n = 0.01 - 0.03$ for sulfo-SMCC. In response to 40-mer DNA attachment, the BSW mode shifts approximately 0.29˚, suggesting an effective refractive index change of approximately $\Delta n = 0.3$ in the region 10 nm above the surface of the BSW sensor. Importantly, the BSW enables detection of large molecules that cannot be detected effectively in most other PSi sensor platforms including waveguides and microcavities. We note that the BSW is not the most sensitive approach for small molecule detection. Concurrently using a Bloch sub-surface wave along with the BSW enables the highest detection sensitivity for small and large molecules, respectively, as detailed in Ref. 32.

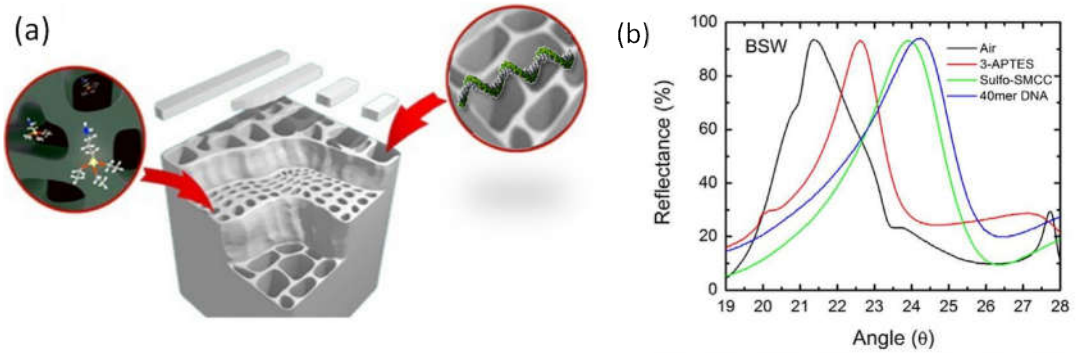

Figure 3. (a) Schematic illustration of the sensing experiment in which small and large species are exposed to a PSi-BSW sensor. Adapted with permission from G. A. Rodriguez, J. D. Lonai, R. L. Mernaugh and S. M. Weiss, *Nanoscale Res. Lett.* 2014, 9, 383. Copyright 2014 Springer. (b) Angle-resolved reflectance spectra after small and large molecule attachment in PSi-BSW. Adapted with permission from G. A. Rodriguez, J. D. Ryckman, Y. Jiao and S. M. Weiss, *Biosens. Bioelectron.* 2014, 53, 486. Copyright 2014 Elsevier B.V.

3.3 PSi ring resonator for highly sensitive biosensing

While PSi microcavities and BSW structures operate with light incident from out-of-plane, some applications benefit from on-chip integration that requires in-plane light propagation. SOI microrings have been demonstrated as highly sensitive sensors that can be easily multiplexed on-chip for high-throughput multi-analyte detection.[33] With its increased surface area, the PSi ring resonator can exhibit the same advantages as an SOI microring while further enhancing the small molecule detection sensitivity due to its large internal active sensing surface area into which molecules can directly interact with the guided mode. In order to determine the bulk sensitivity of PSi rings, salt water solutions of different concentrations were placed on PSi rings of 10 μm radius.[13] Transmission spectra of the ring resonator were measured after 7.5 μL of each salt water solution were placed on the PSi ring. Between each salt water measurement, the PSi ring was rinsed with deionized water until its resonant wavelengths returned to their initial values, ensuring no salt was left behind in the rings. The shift of the PSi ring resonance in response to a given salt water concentration was referenced to the resonance shift of the PSi ring upon exposure to deionized water. As shown in Figure 4a, the bulk sensitivity of the 10 μm radius PSi ring is approximately 384 nm/RIU, which is more than twice as sensitive as typical SOI ring resonator sensors.

The surface sensitivity of the PSi rings was evaluated by specific detection of target peptide nucleic acid (PNA) molecules.[13] Functionalization with 3-APTES, succinimidyl 3-(2-pyridyldithio) propionate (SPDP), and thiol-modified probe DNA (5′-TAG CTA TGG TCC TCG T-3′) was carried out to prepare the PSi rings for detection of 500 nM 16-mer complimentary PNA (ACG AGG ACC ATA GCT A) in deionized water. An excess of 100 μM probe DNA was used to ensure sufficiently high surface density of immobilized probe molecules to maximize target capture. As shown in Figure 4b, the 10 μm radius PSi ring (FSR ~ 19 nm) exhibits resonance shifts of 11 and 2 nm upon the attachment of the 100 μM probe DNA and 500 nM target PNA, respectively. Based on the PNA sensing results, the surface sensitivity of PSi ring resonators is calculated to be approximately 4 pm/nM for the detection of nucleic acid, which is an order of magnitude higher than ring resonator sensors on SOI substrates. However, when detecting large index changes, the resonance of PSi rings may shift by more than one FSR, confounding quantification of the resonance shift in a drop and dry measurement scheme. This FSR challenge can be solved either by integrating microfluidics for continuous real-time measurement or by using a photonic crystal nanobeam configuration that only allows a single mode.[34]

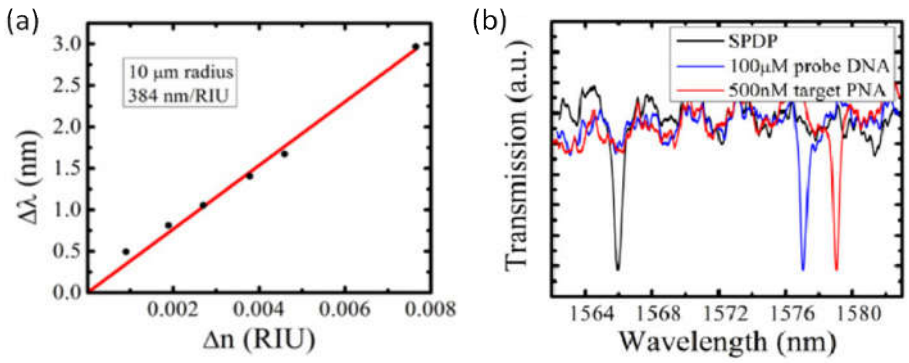

Figure 4. (a) Bulk sensitivity of 10 μm radius PSi ring resonator as determined based on exposure to different salt water concentrations referenced to deionized water. (b) Resonance shifts of 10 μm radius PSi ring due to attachment of DNA and PNA to a SPDP functionalized surface. Adapted with permission from G. A. Rodriguez, S. Hu and S. M. Weiss, *Opt. Express* 2015, 23, 7111. Copyright 2015 Optical Society of America.

3.4 PSi annular Bragg resonator for fluorescence enhancement

For low-cost, point-of-care applications, the drawback of optical resonators such as microrings is the requirement for careful coupling of light in-plane and the costly measurement equipment including a tunable laser and photodetector. Here, we propose to circumvent the need for coupling optics and complex instrumentation by using a PSi-ABR that features its own emission source using cavity coupled QDs that function as built-in light emitters. $AgInS_2/ZnS$ QDs are electrostatically attached to PSi-ABRs following a procedure published previously.[35] Figure 5a shows a microarray of PSi-ABRs, each comprising 55 radial Bragg mirrors surrounding a central disk of 480 nm radius. The fluorescence intensity map in Figure 5a indicates that the highest enhancement of QD emission exists in the central cavity region, which also has the strongest electric-field confinement. In order to quantitatively determine the fluorescence enhancement, PL spectra are measured from QDs in the central cavity region of PSi-ABRs, bare PSi, and a control bare PSi sample with no QD functionalization (Figure 5b). The bare PSi samples are comprised of the same two porous silicon layers that the PSi ABRs have, but the bare samples are not patterned with the ring structures; hence, we expect the surface area for QD binding is larger in the bare PSi samples. The enhancement factor (EF) is calculated by

$$EF = \frac{I_{sample} - I_{background}}{I_{substrate} - I_{background}}$$

where I_{sample}, $I_{substrate}$, and $I_{background}$ refer to the integrated area underneath the PL spectra collected from the QDs in PSi-ABR, bare PSi, and background signals of a bare PSi substrate without QDs.[36] In this work, the enhancement factor is not normalized to the estimated number of QDs contributing to the measured PL. Accordingly, we expect the reported enhancement factor to be a lower bound value. The calculated EF is approximately 7. The EF can be further improved by optimizing the ABR design to obtain a higher quality factor and better alignment of the cavity resonance with the QD emission wavelengths. The PSi-ABR platform integrated with QDs can also function as a label-free sensor requiring straightforward excitation by an inexpensive laser pointer to provide a cavity modified QD emission with strong PL intensities. Any changes to the environmental refractive index of the sensor upon target molecule capture will perturb the cavity resonance conditions, causing a shift in the cavity coupled QD emission spectra. This shift in the QD emission profile can be detected as color change using a camera.

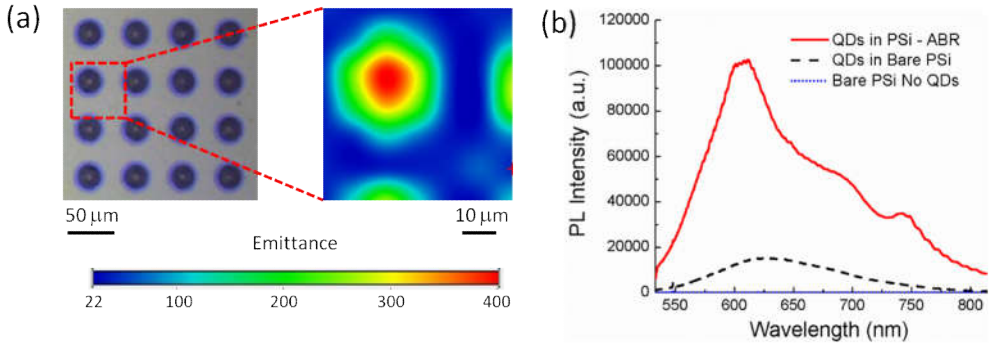

Figure 5. (a) Optical microscope image of a 4×4 microarray of PSi-ABRs. Zoom-in color map shows the distribution of QD emission intensity on a single PSi-ABR. (b) Photoluminescence spectra from QDs adsorbed in PSi-ABR and bare PSi along with a control PSi sample with no QD functionalization.

4. CONCLUSION

The ability to create advanced photonic structures in PSi allows the development of novel optical biosensors that show great promise for future lab-on-chip and sensor array devices. The porous morphology promotes direct light-matter interaction of confined optical modes with molecules that infiltrate the pores. The open-ended PSi membrane overcomes mass transport limitations facing traditional PSi microcavity designs. The PSi BSW enables detection of molecules that exceed the pore size of PSi sensors. The PSi ring resonator exhibits a 40-fold sensitivity improvement over nonporous SOI ring resonators. QD-coupled PSi-ABRs open the door to a low-cost, portable, and highly sensitive label-free colorimetric sensing platform.

ACKNOWLEDGEMENTS

This work was funded in part by the Army Research Office (W911NF-15-1-0176 and W911NF-09-1-0101) and National Science Foundation (ECCS-0746296). Lithography was conducted at the Center for Nanophase Materials Science (CNMS) at Oak Ridge National Laboratory, which is a DOE Office of Science User Facility. Additional fabrication and characterization were carried out at the Vanderbilt Institute for Nanoscale Science and Engineering (VINSE) and Vanderbilt Institute for Integrative Biosystem Research and Education (VIIBRE). Graham acknowledges the NSF-REU program at Vanderbilt (DMR-1263182).

REFERENCES

[1] Jane, A., Dronov, R., Hodges, A., and Voelcker, N. H., "Porous silicon biosensors on the advance," Trends Biotechnol. 27(4), 230-239 (2009).

[2] Gupta, B., Zhu, Y., Guan, B., Reece, P. J., and Gooding, J. J., "Functionalised porous silicon as a biosensor: Emphasis on monitoring cells in vivo and in vitro," Analyst 138(13), 3593-3615 (2013).

[3] Harraz, F. A., "Porous silicon chemical sensors and biosensors: A review," Sens. Actuator B-Chem. 202, 897-912 (2014).

[4] Janshoff, A., Dancil, K.-P. S., Steinem, C., Greiner, D. P., Lin, V. S. Y., Gurtner, C., Motesharei, K., Sailor, M. J., and Ghadiri, M. R., "Macroporous p-Type silicon Fabry−Perot layers. Fabrication, characterization, and applications in biosensing," J. Am. Chem. Soc. 120(46), 12108-12116 (1998).

[5] Jalkanen, T., Torres-Costa, V., Salonen, J., Bjorkqvist, M., Makila, E., Martinez-Duart, J. M., and Lehto, V. P., "Optical gas sensing properties of thermally hydrocarbonized porous silicon Bragg reflectors," Opt. Express 17(7), 5446-5456 (2009).

[6] Ilyas, S., Bocking, T., Kilian, K., Reece, P. J., Gooding, J., Gaus, K., and Gal, M., "Porous silicon based narrow line-width rugate filters," Opt. Mater. 29(6), 619-622 (2007).
[7] Ouyang, H., Christophersen, M., Viard, R., Miller, B. L., and Fauchet, P. M., "Macroporous silicon microcavities for macromolecule detection," Adv. Funct. Mater. 15(11), 1851-1859 (2005).
[8] Krismastuti, F. S. H., Pace, S., and Voelcker, N. H., "Porous silicon resonant microcavity biosensor for matrix metalloproteinase detection," Adv. Funct. Mater. 24(23), 3639-3650 (2014).
[9] Rong, G., Najmaie, A., Sipe, J. E., and Weiss, S. M., "Nanoscale porous silicon waveguide for label-free DNA sensing," Biosens. Bioelectron. 23(10), 1572-1576 (2008).
[10] Zhao, Y. L., Lawrie, J. L., Beavers, K. R., Laibinis, P. E., and Weiss, S. M., "Effect of DNA-induced corrosion on passivated porous silicon biosensors," ACS Appl. Mater. Inter. 6(16), 13510-13519 (2014)
[11] Qiao, H., Guan, B., Gooding, J. J., and Reece, P. J., "Protease detection using a porous silicon based Bloch surface wave optical biosensor," Opt. Express 18(14), 15174-15182 (2010).
[12] Guillermain, E., Lysenko, V., Orobtchouk, R., Benyattou, T., Roux, S., Pillonnet, A., and Perriat, P., "Bragg surface wave device based on porous silicon and its application for sensing," Appl. Phys. Lett. 90(24), 241116 (2007).
[13] Rodriguez, G. A., Hu, S. R., and Weiss, S. M., "Porous silicon ring resonator for compact, high sensitivity biosensing applications," Opt. Express 23(6), 7111-7119 (2015).
[14] Girault, P., Lorrain, N., Lemaitre, J., Poffo, L., Guendouz, M., Hardy, I., Gadonna, M., Gutierrez, A., Bodiou, L., and Charrier, J., "Racetrack micro-resonators based on ridge waveguides made of porous silica," Opt. Mater. 50, 167-174 (2015).
[15] White, I. M., and Fan, X. D., "On the performance quantification of resonant refractive index sensors," Opt. Express 16(2), 1020-1028 (2008).
[16] Sirbuly, D. J., Tao, A., Law, M., Fan, R., and Yang, P. D., "Multifunctional nanowire evanescent wave optical sensors," Adv. Mater. 19(1), 61-66 (2007).
[17] Ouyang, H., Striemer, C. C., and Fauchet, P. M., "Quantitative analysis of the sensitivity of porous silicon optical biosensors," Appl. Phys. Lett. 88(16), 163108 (2006).
[18] Wei, X., Kang, C., Liscidini, M., Rong, G., Retterer, S. T., Patrini, M., Sipe, J. E., and Weiss, S. M., "Grating couplers on porous silicon planar waveguides for sensing applications," J. Appl. Phys. 104(12), 123113 (2008).
[19] Pacholski, C., "Photonic Crystal Sensors Based on Porous Silicon," Sensors 13(4), 4694-4713 (2013).
[20] Rong, G., Ryckman, J. D., Mernaugh, R. L., and Weiss, S. M., "Label-free porous silicon membrane waveguide for DNA sensing," Appl. Phys. Lett. 93(16), 161109 (2008).
[21] Wei, X., and Weiss, S. M., "Guided mode biosensor based on grating coupled porous silicon waveguide," Opt. Express 19(12), 11330-11339 (2011).
[22] Zhao, Y., Gaur, G., Mernaugh, R. L., Laibinis, P. E., and Weiss, S. M., "Comparative kinetic analysis of closed-ended and open-ended porous sensors," Nanoscale Res. Lett. 11(1), 395 (2016).
[23] Zhao, Y. L., Gaur, G., Retterer, S. T., Laibinis, P. E., and Weiss, S. M., "Flow-through porous silicon membranes for real-time label-free biosensing," Anal. Chem. 88(22), 10940-10948 (2016).
[24] Rodriguez, G. A., Ryckman, J. D., Jiao, Y., and Weiss, S. M., "A size selective porous silicon grating-coupled Bloch surface and sub-surface wave biosensor," Biosens. Bioelectron. 53, 486-493 (2014).
[25] Liscidini, M., and Sipe, J. E., "Analysis of Bloch-surface-wave assisted diffraction-based biosensors," J. Opt. Soc. Am. B. 26(2), 279-289 (2009).
[26] Bogaerts, W., De Heyn, P., Van Vaerenbergh, T., De Vos, K., Selvaraja, S. K., Claes, T., Dumon, P., Bienstman, P., Van Thourhout, D., and Baets, R., "Silicon microring resonators," Laser Photonics Rev. 6(1), 47-73 (2012).
[27] Scheuer, J., and Yariv, A., "Annular Bragg defect mode resonators," J. Opt. Soc. Am. B. 20(11), 2285-2291 (2003).
[28] Scheuer, J., Green, W. M. J., DeRose, G., and Yariv, A., "Low-threshold two-dimensional annular Bragg lasers," Opt. Lett. 29(22), 2641-2643 (2004).
[29] Scheuer, J., Green, W. M. J., DeRose, G. A., and Yariv, A., "Lasing from a circular Bragg nanocavity with an ultrasmall modal volume," Appl. Phys. Lett. 86(25), 251101 (2005).
[30] Gaur, G., Koktysh, D. S., and Weiss, S. M., "Immobilization of quantum dots in nanostructured porous silicon films: Characterizations and signal amplification for dual-mode optical biosensing," Adv. Funct. Mater. 23(29), 3604-3614 (2013).

[31] Lawrie, J. L., Yang, J., and Weiss, S. M., "Size-dependent infiltration and optical detection of nucleic acids in nanoscale pores," IEEE Trans. Nanotechnol. 9(5), 596-602 (2010).
[32] Rodriguez, G. A., Lonai, J. D., Mernaugh, R. L., and Weiss, S. M., "Porous silicon Bloch surface and sub-surface wave structure for simultaneous detection of small and large molecules," Nanoscale Res. Lett. 9(1), 383 (2014).
[33] Qavi, A. J., Mysz, T. M., and Bailey, R. C., "Isothermal discrimination of single-nucleotide polymorphisms via real-time kinetic desorption and label-free detection of DNA using silicon photonic microring resonator arrays," Anal. Chem. 83(17), 6827-6833 (2011).
[34] Rodriguez, G. A., Markov, P., Cartwright, A. P., Retterer, S. T., Kravchenko, I. I., and Weiss, S. M., "Photonic crystal nanobeam biosensors based on porous silicon," Manuscript in Preparation, (2017).
[35] Gaur, G., Koktysh, D. S., Fleetwood, D. M., Weller, R. A., Reed, R. A., and Weiss, S. M., "Influence of interfacial oxide on the optical properties of single layer CdTe/CdS quantum dots in porous silicon scaffolds," Appl. Phys. Lett. 107(6), 063106 (2015).
[36] Liu, Y. M., Wang, S., Park, Y. S., Yin, X. B., and Zhang, X., "Fluorescence enhancement by a two-dimensional dielectric annular Bragg resonant cavity," Opt. Express 18(24), 25029-25034 (2010).